J Mater Sci (2011) 46:2064–2070
DOI 10.1007/s10853-010-5039-6

Property-processing relations in developing thermoelectric ceramics: $Na_{1-x}Co_2O_4$

Hiroo Yamakawa · Soonil Lee · Hiroshi Takagi · Clive A. Randall

Received: 30 April 2010 / Accepted: 29 October 2010 / Published online: 12 November 2010
© Springer Science+Business Media, LLC 2010

Abstract Polycrystalline $Na_{1-x}Co_2O_4$ is a promising *p*-type oxide thermoelectric, and it was investigated in a property-processing study to enhance the thermoelectric properties for high temperature applications. The density of the ceramics was improved by a post-milling process, and consequently, we obtained better thermoelectric power factors (PF) due to an associated improvement in electrical conductivity. Through a milling process, and sintering at 1203 K, we obtained an enhanced thermoelectric power factor of $\sim$4 μW/cm K^2 at 500 K for randomly orientated polycrystalline ceramics. The Seebeck coefficient variation with temperature demonstrates through modeling that the conduction mechanism changed from metallic to a semiconducting behavior between temperatures 300 to 400 K.

Introduction

For several decades, thermoelectric materials have been studied for directly converting thermal energy into electrical energy. Thermoelectric devices can work over a wide temperature range and utilize waste heat from various sources, e.g., geothermal, solar-thermal, exhaust heat from factories, or automobiles, etc. The conversion efficiency of the thermoelectric devices is mainly determined by the figure of merit of the material. The figure of merit is defined as $ZT = S^2\sigma T/k$ [1], where S is the Seebeck coefficient, σ is the electrical conductivity, and k is the thermal conductivity. These values are directly related to the efficiency of a thermoelectric module, i.e., higher ZT yields higher energy conversion efficiencies. For practical applications, it is generally required that $ZT \geq 1$, and this is a challenge to the discipline [2, 3].

Most thermoelectric modules consist of semiconductor alloys, which are expensive to manufacture and become unstable at high temperatures [2]. Oxide materials, which are more stable, less toxic, and lower in cost, could potentially replace these semiconductors and expand the industry from niche to major markets. Recently, some *p*-type and *n*-type oxide thermoelectric materials have been reported, but they suffer from low figure of merit values. One of the promising *p*-type materials is based on non-stoichiometric sodium cobalt oxides. Terasaki et al. [4] reported that $NaCo_2O_4$ single crystal shows relatively high ZT value 0.75 at 300 K. After this study, many efforts were focused on developing the sodium cobalt oxides, selections of the reported data is shown in Table 1.

In terms of the cost efficiency and feasibility of fabrication, polycrystalline $NaCo_2O_4$ could be an attractive choice. However, the polycrystalline $NaCo_2O_4$ has lower ZT value than single crystals, due to a lower electrical conductivity. This is, in part, due to the high anisotropy in conductivity, but also due to the microstructure and stoichiometric variations that can occur. Polycrystalline $NaCo_2O_4$ synthesized by conventional solid-state routes typically shows ZT values 0.01–0.11 [6, 9]. On the other hand, nonstoichiometric materials, such as $Na_{1.7}Co_2O_4$ polycrystalline prepared by a chemical solution process [polymerized complex (PC) method], showed higher ZT value of 0.8 at 955 K and $\sim$0.22 at 500 K [7]. For this study, we wish to make a direct comparison to single crystals of $NaCo_2O_4$ and avoid the issues of nonstoichiometric compositions. The challenge of

H. Yamakawa · S. Lee (✉) · C. A. Randall
Center for Dielectric Studies, Materials Research Institute, The Pennsylvania State University, University Park, PA 16802, USA
e-mail: leesoonil@gmail.com

H. Yamakawa · H. Takagi
Murata Manufacturing Co. Ltd, 10-1 Higashikotari 1-chome, Nagaokakyo, Kyoto 617-8555, Japan

Table 1 Comparison of thermoelectric properties in sodium cobalt oxide based *p*-type oxides

	S (μV/K)	ρ (=1/σ) (Ω cm)	κ (W/mK)	P.F. = S^2/ρ (μW/cm K^2)	ZT	Temp. (K)	Ref.
Single crystal $NaCo_2O_4$	100	0.0002	–	50.0	–	300	[4]
$Na_{1.3}Co_2O_4$	5	0.0065	–	0.47	–	300	[5]
$NaCo_{1.9}Pd_{0.1}O_4$	108	0.009	2.85	1.3	0.045	723	[6]
	88	0.0007	2.88	0.6	0.026	500	
$NaCo_2O_4$	138	0.031	3	0.61	0.0175	723	
	114	0.028	3.2	0.46	0.009	500	
$Na_{1.7}Co_2O_4$ (Texture-like)	208	0.0034	1.62	12.7	0.8	955	[7]
	140	0.00265	1.7	7.4	0.22	500	
$Na_{0.75}CoO_2$	22	0.021	–	0.02	–	45	[8]
$NaCo_2O_4$	212	0.019	2.2	2.4	0.11	973	[9]
	96	0.04	3	0.2	0.004	500	
$Na(Co_{0.9}Cu_{0.1})_2O_4$	440	0.006452		30.8	–	1073	[10]
	260	0.005128		13		723	
$Na_{1.5}Co_{1.8}Ag_{0.2}O_4$	170	0.0095	2.4	3.042	0.124	973	[11]
	100	0.0070	2.4	1.8	0.03	500	
$La_{0.9}Na_{0.1}CoO_3$	100	0.02	1.55	0.5	0.01	575	[12]
	130	0.13	1.2	0.13		500	
$Li_{0.25}Na_{0.15}CoO_2$	45	0.03	–	0.0675	–	300	[13]
$Li_{0.40}Na_{0.18}CoO_2$	96	0.21	–	0.0439	–	300	
$Na_{0.78}CoO_2$	200	0.0025	–	16.0	–	1050	[14]
	130	0.0020		8.5		500	
$Na_{0.71}Co_{0.7}Ru_{0.3}O_4$	165	0.08	–	0.340	–	300	[15]
$Na_xCo_2O_4$	177	0.0074	–	4.3	–	850	[16]
	100	0.0063		1.6		500	
Textured $Na_xCoO_{2-\delta}$	137	0.0054	–	3.5	–	800	[17]
	100	0.0042		2.4		550	
$Na_{1-x}Co_2O_4$	160	0.0077	–	4.0	–	500	This study

P.F. thermoelectric power factor

fabricating polycrystalline $NaCo_2O_4$ through conventional solid-state methods is that it shows a rather low density $<\sim 80\%$. In this study, we introduce a processing approach within solid-state methodology that can improve the thermoelectric power factor (PF) value of $NaCo_2O_4$. This article will discuss microstructure, density, and thermoelectric power factor for this solid-state approach.

Experimental procedure

The polycrystalline $Na_{1-x}Co_2O_4$ was fabricated by a conventional solid-state process. The starting materials were carbonate Na_2CO_3 (ACS primary standard, 99.95–100.05%, Alfa Aesar) and oxide Co_3O_4 (99.7%, Alfa Aeser), used for the solid-state process [10]. The Na_2CO_3 and Co_3O_4 powders are mixed in ethyl alcohol and ball milling for 6 h with ZrO_2 media. The slurry was dried at 393 K for 12 h. The mixed powders were then calcined in an alumina crucible at 1073 and 1123 K for 12 h three times, with intermittent grinding, and with addition of 10 mol% excess Na_2CO_3 [18], considering the Na volatility based on TGA analysis. Thermal decomposition was monitored with a Thermogravimetric Analysis (TGA: SDT 2960, TA Instruments, New Castle, DE). The calcined powders were then ground carefully with mortar and pestle, and then passed through a 200-mesh sieve. Subsequently, the calcined powders were uniaxially pressed in a die of 12.7-mm diameter and then pressed under cold isostatic pressure (CIP) at 200 MPa. The pellets were sintered in air at 1173, 1203, 1233, and 1263 K for 12 h. Figure 1 shows a schematic of the basic solid-state process used to produce precursor powders.

The particle size of the milled powders was analyzed by laser scattering particle size distribution analyzer (ZETA SIZER, Malvern Instruments Ltd). X-ray diffraction (XRD, PAD V, Scintag Inc) analysis was used to determine the crystalline phase using ground powder from sintered samples. Scans were taken using Cu Kα radiation over the range from $2\theta = 10^{\circ}$ to 70°.

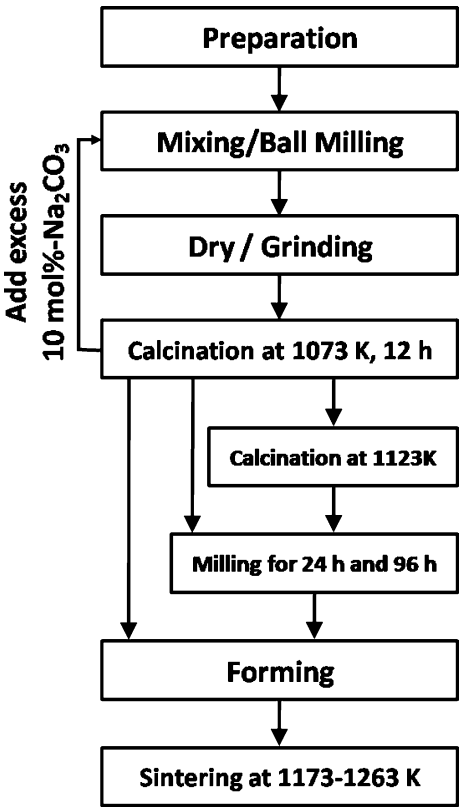

Fig. 1 A schematic flowchart of experimental procedure for $Na_{1-x}Co_2O_4$ synthesis

Grain size and morphology were determined using a scanning electron microscope (SEM, S-3500N, HITACHI). The samples for the Seebeck coefficient (Thermopower) were cut from the pellets into rectangular bars of ca. $4.5 \times 1.5 \times 0.8$ mm^3. Seebeck coefficients were measured in a MMR Technology Inc. SB-100 Programmable Seebeck Controller from 200 to 600 K in a vacuum below 5 mTorr. The electrical conductivity versus temperature was measured with a HP 4284A LCR meter at 20 Hz from 200 to 525 K using a four-probe method.

Results and discussion

The result of the TGA and DSC measurements for a powder of $Na_{1-x}Co_2O_4$ after three times calcinations at 1073 K is represented in Fig. 2a. Even after calcination process, the TGA data still show weight loss about 10%. The majority of this is due to the volatile Na between 900 and 1175 K. The first region, from 300 to 600 K, is removal of moisture, and the high temperature weight loss and endothermic reaction are associated with decomposition of Co_3O_4 to CoO. The overall reaction for $NaCo_2O_4$ phase formation is as follows [19], considering the Na vaporization:

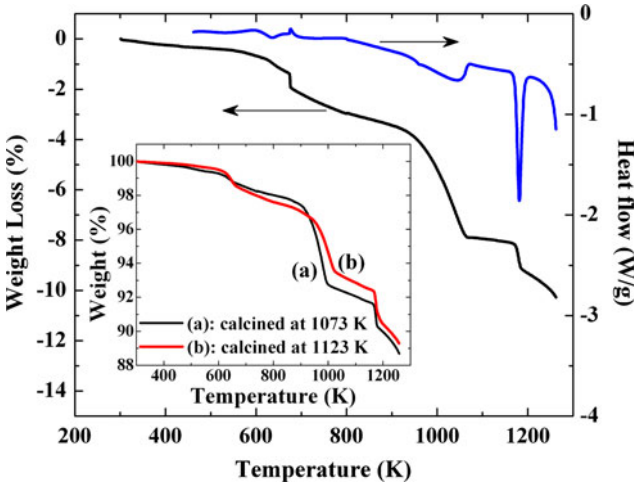

Fig. 2 TGA/DSC curves after three-time calcinations at 1073 K. The *inset* is the TGA curves of powders calcined at 1073 and 1123 K as a function of temperature

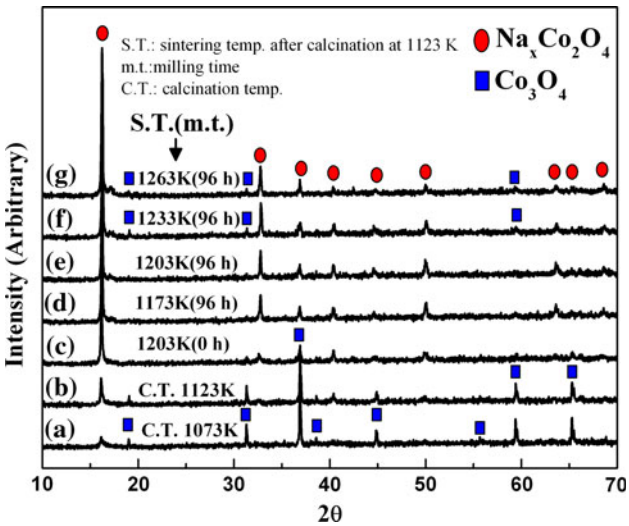

Fig. 3 Powder x-ray diffraction patterns of samples calcined at 1073 and 1123 K (*a* and *b*), sintered at 1203 K without second milling (*c*), and sintered at 1173, 1203, 1233, and 1263 K after second milling for 96 h: *d*, *e*, *f*, and *g*, respectively

$$\frac{1}{2}Na_2CO_3(s) + \frac{2}{3}Co_3O_4(s) + \frac{5}{12}O_2(g) \longrightarrow Na_{1-x}Co_2O_4(s) + \frac{1}{2}CO_2(g) + xNa(g) \quad (1)$$

Figure 3 shows XRD patterns after calcinations and sintering with different temperatures and milling times. After calcination at 1073 and 1123 K, there were mainly two phases: $Na_{1-x}Co_2O_4$ and Co_3O_4 phases. At 1123 K, the volume ratio of $Na_{1-x}Co_2O_4$ phase slightly increased, but the Co_3O_4 phase is still the main phase. The $Na_{1-x}Co_2O_4$ phase was formed dominantly after sintering above 1173 K with small amount of the Co_3O_4 phase created due to the evaporation of Na.

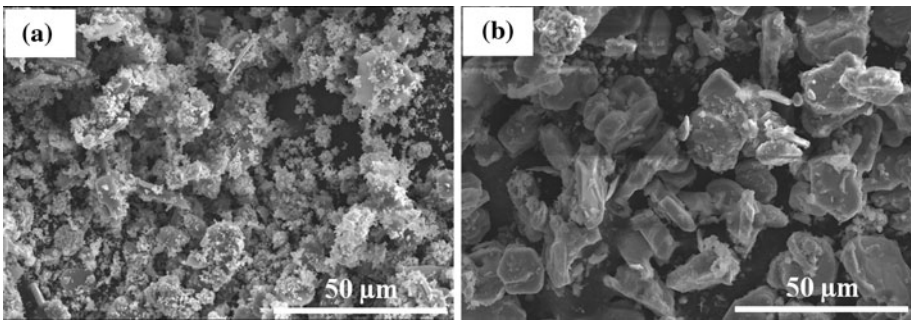

Fig. 4 SEM images of powders calcined at (**a**) 1073 K and (**b**) 1123 K for 12 h in air

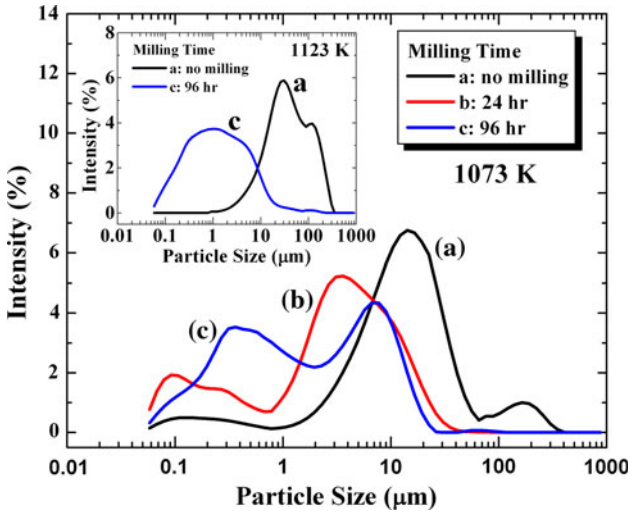

Fig. 5 Particle size distribution of powders calcined at 1073 and 1123 K (*inset*) with different milling time: 0 (*a*), 24 (*b*), and 96 (*c*) h

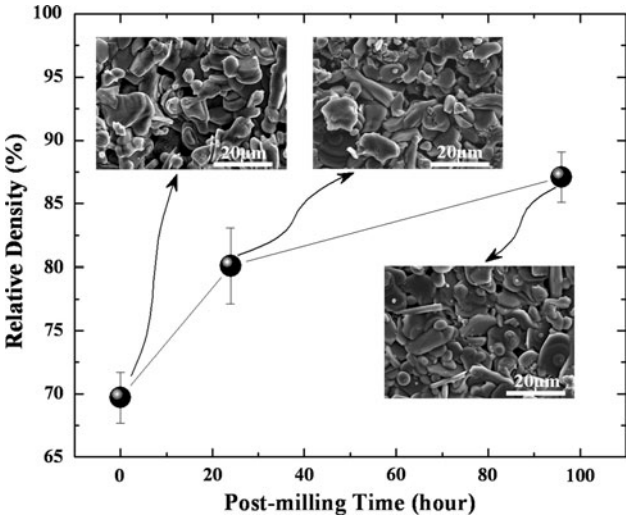

Fig. 6 Relative density and microstructure as a function of milling time. The samples were calcined at 1070 K and milled for 0, 24, and 96 h, respectively, before being sintered at 1203 K in air

Figure 4 shows the SEM images obtained from powders of the mixed phases ($Co_3O_4 + Na_{1-x}Co_2O_4$) after calcinations at 1073 and 1123 K. In comparing SEM images, the particle size of the powders calcined at 1123 K is larger than that of powders calcined at 1073 K, as would be expected. Figure 5 shows the particle size distribution of the powders calcined at 1073 K with different milling times of 0, 24, and 96 h. The post-milling process reduced the particle size, and consequently, the relative density also increased with milling time with almost constant grain size, as shown in Fig. 6. Figure 6(inset) shows the SEM images from the surface of the sintered bulk samples, and, as expected, the samples with longer milling time showed less porosity.

Through improved densification, the electrical conductivity increased significantly, whereas the Seebeck coefficient, showing positive value with *p*-type charge carrier, did not vary significantly, as shown in Fig. 7a and b. As a result, the thermoelectric power factor was enhanced, as shown in Fig. 7c. Furthermore, it is noted that the power factor increases with increasing temperature due to the increase in the Seebeck coefficient. The electrical conductivity data show a metallic behavior ($d\sigma/dT < 0$), but

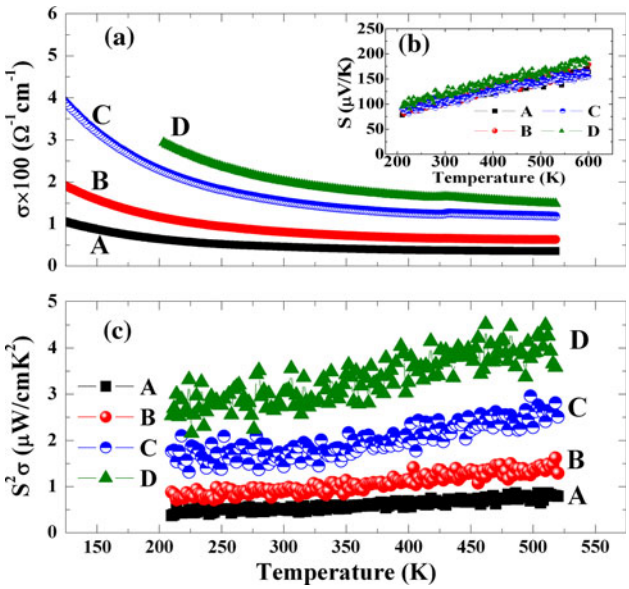

Fig. 7 Electrical conductivity (**a**), Seebeck coefficient (**b**), and thermoelectric power factor (**c**) as a function of temperature of samples with different milling times (*A*: 0 h, *B*: 24 h, *C*: 96 h, and *D*: 96 h). Samples were calcined at 1073 K (samples *A*, *B*, and *C*) and 1123 K (sample *D*), and then sintered at 1203 K in air

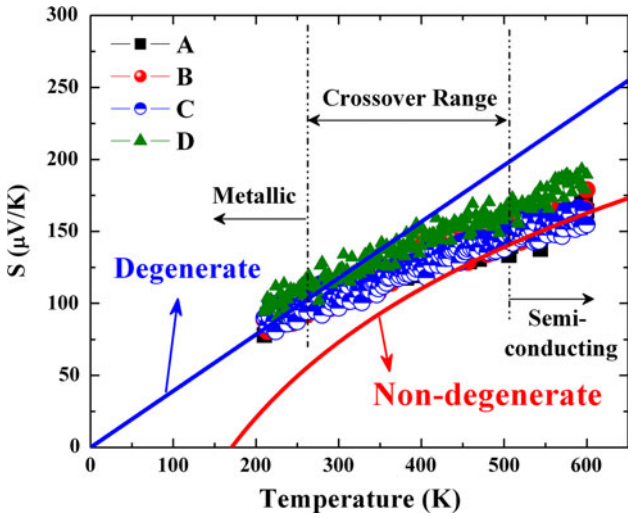

Fig. 8 Seebeck coefficient as a function of temperature for samples *A*, *B*, *C*, and *D*. The *solid lines* were fitted with Eqs. 2 and 3 for degenerate Fermi gas model and non-degenerate semiconductor model, respectively

the Seebeck coefficient presents both metallic and non-degenerate semiconducting behavior (see Fig. 8). The Seebeck coefficient has a temperature dependence that can be described in terms of a degenerate Fermi gas model for metallic behavior [20–23],

$$S = \left(\frac{8\pi^{8/3}k_B^2}{3^{5/3}h^2e}\right)m * n_p^{-2/3}T, \tag{2}$$

and a non-degenerate semiconductor model for semiconducting behavior [23, 24],

$$S = k_B/e\left[\ln\left(N_V/n_p\right) + A\right], \tag{3}$$

where m^* is the hole effective mass, n_p is the carrier concentration, k_B is the Boltzmann constant, h is the Plank's constant, N_v is the effective density of states in the valence band, and A is the carrier transport or scattering factor. As shown in Fig. 8, in which the fitting was done by adjusting relatively the effective mass and carrier concentration at low temperature below 250 K, the Seebeck coefficient shows a metallic behavior. However, with increasing temperature, the Seebeck coefficient deviates from the degenerate Fermi gas model, and then starts to show a non-degenerate semiconducting trend at high temperature above 500 K. Therefore, the entire Seebeck coefficient data presents an intermediate between metallic and semiconducting behavior. In this study, with polycrystalline $Na_{1-x}Co_2O_4$, the crossover temperature did not match between electrical conductivity and Seebeck coefficient; the electrical conductivity shows a metallic behavior over the observed temperature range, while the metallic behavior of Seebeck coefficient starts to deviate above 250 K. Although complete Seebeck and resistivity anisotropic data do not exist in the literature, there are important trends that are noted in the work of Terasaki et al. [4]. For example, at low temperatures, the Seebeck and resistivity temperature dependence shows metallic behavior for the *a*-direction of the $NaCo_2O_4$ structure. At high temperatures in the *c*-direction, there is a crossover from metallic to semiconducting. Unfortunately, there does not exist equivalent *c*-direction data in the Seebeck data owing to the difficulty of the crystal morphology. Our analysis of the polycrystalline case indicates the crossover between the metallic to semiconducting behavior. We, therefore, expect complex transport process between different directions that can dominate in different temperature regimes, such as those concepts of incoherent hopping in layered structures, as proposed by Yoshida et al. [25] in Sr_2RuO_4. If this is the case, a decoupling reflects itself through changes in the temperature dependence of Seebeck coefficient and electrical resistivity. Recently, we have observed a decoupling between electrical conductivity and Seebeck coefficient in randomly oriented ceramics composed of highly reduced, perovskite structured $SrTiO_{3-\delta}$ and $BaTiO_{3-\delta}$. In these materials "wormhole"-like defects in the grains gave rise to a decoupling of temperature variation in the electrical conductivity and the Seebeck coefficient [23]. In this study, the Seebeck coefficient of randomly oriented polycrystalline $Na_{1-x}Co_2O_4$ in the temperature range measured does not show a polaron hopping mechanism having a temperature invariant Seebeck coefficient ($S = (k_B/e)\ln[(2\text{-}c)/c]$[26, 27], where c can be the $[Co^{2+}]/[Co^{3+}]$. Once again, the crystal anisotropic properties in randomly oriented ceramic give rise to this uncertainty in determining the conduction mechanism. This requires further investigation at higher temperatures and detailed studies to determine cation valence and stoichiometric distributions.

The processing adopted in this article lead to improvements in densification and microstructure and in turn the magnitude of the thermoelectric power factor. Figure 9 shows the relative density variation and the corresponding microstructures of the ceramics calcined at 1123 K and then sintered at 1173, 1203, 1233, and 1263 K. In general, the ceramics calcined at 1123 K showed higher density than ceramics calcined at 1073 K. Less volatile sodium from precursors during sintering for the samples calcined at higher temperatures are believed to account for this improvement (see Fig. 2(inset)). The relative density increased with increasing temperature, and the grain size increased for the 1233 and 1263 K sintering conditions. In Fig. 10, the electrical conductivity and thereby power factor increased up to 1203 K and then decreased with increasing sintering temperature. This may result from the volatility of sodium at high temperature; the XRD data show a small amount of Co_3O_4 phase in the samples

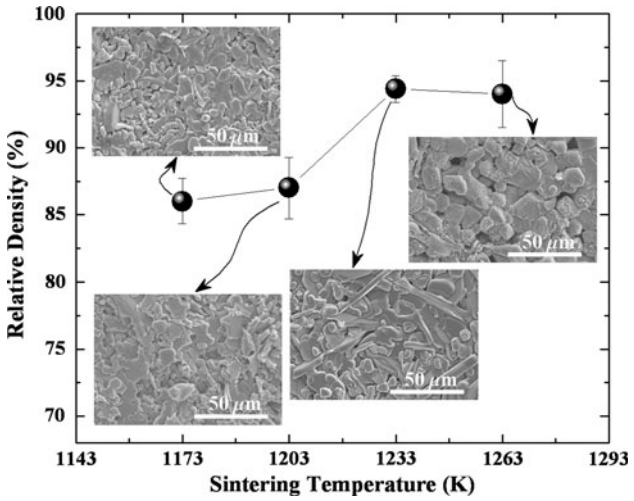

Fig. 9 Relative density variation and SEM images as a function of sintering temperature. The samples were calcined at 1123 K and sintered at 1173, 1203, 1233, and 1263 K in air

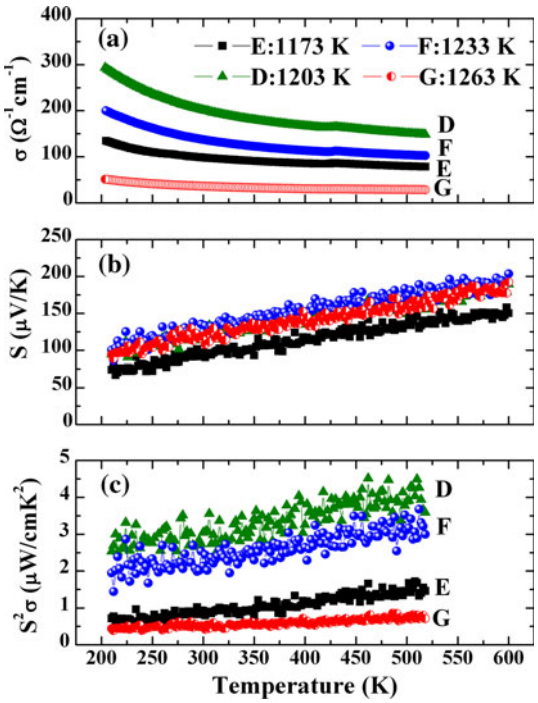

Fig. 10 Electrical conductivity (**a**), Seebeck coefficient (**b**), and thermoelectric power factor (**c**) as a function of temperature. The samples were calcined at 1123 K and sintered at 1173 K (*E*), 1203 K(*D*), 1233 K(*F*), and 1263 K (*G*) for 12 h in air

sintered at 1233 and 1263 K (see Fig. 3); the relative peak intensity of the Co_3O_4 phase at above 1233 K is slightly higher than below 1203 K. Ito et al. [7] also reported that the amount of Co_3O_4 phase increases with decreasing x in $Na_xCo_2O_4$. It is anticipated that the Co_3O_4 phase, which has a lower conductivity, decreased the entire electrical conductivity due to the carrier trapping at the phases or inter-phases. The sintering at 1203 K showed the best conditions in terms of the relative density, phase-purity, and grain morphology. As would be expected, these gave rise to the enhancement of thermoelectric power factor due to mainly the increase of electrical conductivity. Regardless of the sintering temperature, all samples showed an increase of thermoelectric power factor with temperature.

Summary and conclusions

In conclusion, polycrystalline $Na_{1-x}Co_2O_4$ was investigated to enhance the thermoelectric properties in a solid-state process. The relative density was improved by post-milling process and resulted in better thermoelectric power factor, due to mainly the electrical conductivity improvement. The optimum sintering temperature with respect to the density, phase stability, and grain morphology was determined to be 1203 K, showing the enhanced thermoelectric power factor ~ 4 μW/cm K^2 at 500 K, which is high compared to the literature values reported for other randomly orientated polycrystalline $Na_xCo_2O_4$. This demonstrates that with both optimal control of Na volatility and texture, high performance $NaCo_2O_4$ can be produced.

It is also noted that the conduction mechanism changes from metallic to semiconducting behavior with increasing temperature, based on the Seebeck coefficient variation with temperature, indicating higher power factor can be reached at higher temperature.

Acknowledgements This study is based upon work supported by the National Science Foundation, as part of the Center for Dielectric Studies under Grant No. 0628817. The authors wish to acknowledge the CDS membership and NSF I/UCRC program for support on this topic.

References

1. Goldsmid HJ (1964) Thermoelectric refrigeration. Plenum press, New York
2. Ohta H, Mune Y, Koumoto K, Mizoguchi T, Ikuhara Y (2008) Thin Solid Films 516:5916
3. Snyder GJ, Toberer ES (2008) Nat Mater 7:105
4. Terasaki I, Sasago Y, Uchinokura K (1997) Phys Rev B 56:R12685
5. Kawata T, Iguchi Y, Itoh T, Takahata K, Terasaki I (1999) Phys Rev B 60:10584
6. Kurosaki K, Muta H, Uno M, Yamanaka S (2001) J Alloys Compd 315:234
7. Ito M, Nagira T, Furumoto D, Katsuyama S, Nagai H (2003) Scr Mater 48:403
8. Motohashi T, Ueda R, Naujalis E, Tojo T, Terasaki I, Atake T, Karppinen M, Yamauchi H (2003) Physica B 329–333:914
9. Seetawan T, Amornkitbamrung V, Burinprakhon T, Maensiri S, Tongbai P, Kurosaki K, Muta H, Uno M, Yamanaka S (2006) J Alloys Compd 416:291
10. Park K, Jang KU, Kwon HC, Kim JG, Cho WS (2006) J Alloys Compd 419:213

11. Seetawan T, Amornkitbamrung V, Burinprakhon T, Maensiri S, Kurosaki K, Muta H, Uno M, Yamanaka S (2006) J Alloys Compd 414:293
12. He T, Chen J, Calvarese TG, Subramanian MA (2006) Solid State Sci 8:467
13. Bos JWG, Hertz JT, Morosan E, Cava RJ (2007) J Solid State Chem 180:3211
14. Liu P, Chen G, Cui Y, Zhang H, Xiao F, Wang L, Nakano H (2008) Solid State Ion 179:2308
15. Strobel P, Muguerra H, Hebert S, Pachoud E, Colin C, Julien MH (2009) J Solid State Chem 182:1872
16. Zhang L, Tang X, Gao W (2009) J Electron Mater 38:1229
17. Itahara H, Fujita K, Sugiyama J, Nakamura K, Tani T (2003) J Ceram Soc Jpn 111:227
18. Maeda E, Ohtaki M (2000) Trans Mater Res Soc Jpn 25:237
19. Ohtaki M, Shouji K (2005) In: Proceedings of the 24th international conference on thermoelectrics, Kyushu University, Japan, p 472
20. Ashcroft NW, Mermin ND (1976) Solid state physics. Harcourt, Inc, Orlando
21. Goodenough JB (1971) Prog Solid State Chem 5:145
22. Moos R, Gnudi A, Hardtl KH (1995) J Appl Phys 78:5042
23. Lee S, Yang G, Wilke RHT, Trolier-McKinstry S, Randall CA (2009) Phys Rev B 79:134110
24. Cox PA (1992) Transition metal oxides. Oxford University Press, New York, p 158
25. Yoshida K, Maeno Y, Nishizaki S, Ikeda S, Fujita T (1996) J Low Temp Phys 105:1593
26. Heikes RR, Ure RW Jr (1961) Thermoelectricity: science and engineering. Interscience, New York, p 77
27. Chaikin PM, Beni G (1976) Phys Rev B 13:647